

Distribution of basal sliding coefficients under ice sheets

D. Pollard and
R. M. DeConto

A simple inverse method for the distribution of basal sliding coefficients under ice sheets, applied to Antarctica

D. Pollard¹ and R. M. DeConto²

¹Earth and Environmental Systems Institute, Pennsylvania State University, University Park, PA, USA

²Department of Geosciences, University of Massachusetts, Amherst, MA, USA

Received: 26 March 2012 – Accepted: 28 March 2012 – Published: 12 April 2012

Correspondence to: D. Pollard (pollard@essc.psu.edu)

Published by Copernicus Publications on behalf of the European Geosciences Union.

This discussion paper is/has been under review for the journal The Cryosphere (TC). Please refer to the corresponding final paper in TC if available.

Title Page

Abstract

Introduction

Conclusions

References

Tables

Figures

⏪

⏩

◀

▶

Back

Close

Full Screen / Esc

Printer-friendly Version

Interactive Discussion

Abstract

Variations in intrinsic bed conditions that affect basal sliding, such as the distribution of deformable sediment versus hard bedrock, are important boundary conditions for large-scale ice-sheet models, but are hard to observe and remain largely uncertain below the modern Greenland and Antarctic ice sheets. Here a very simple model-based method is described for deducing the modern spatial distribution of basal sliding coefficients. The model is run forward in time, and the basal sliding coefficient at each grid point is periodically increased or decreased depending on whether the local ice surface elevation is too high or too low compared to observed, in areas of unfrozen bed. The method considerably reduces large-scale errors in Antarctic ice elevation, from several 100's to a few 10 m in most regions. Remaining ice elevation errors over mountain ranges such as the Transantarctics are further improved by parameterizing the possible effect of sub-grid topography in the basal sliding law, representing sliding in deep valleys. Results are briefly compared with previous work using relatively sophisticated control methods, and the method is applied to alternate topographies of the Recovery Glacier basin.

1 Introduction

One major uncertainty in modeling continental ice sheets is the distribution of bed properties that determine the rate of sliding at the ice-bed interface. Basal sliding over hard beds is commonly described by a law relating sliding velocity u_b to the basal shear stress τ_b , such as

$$u_b = C(x, y)N^{-q}\tau_b^n \quad (1)$$

where C is a basal sliding coefficient that depends on intrinsic bed properties such as small-scale roughness, and N is the effective pressure, i.e., ice overburden not

TCD

6, 1405–1444, 2012

Distribution of basal sliding coefficients under ice sheets

D. Pollard and
R. M. DeConto

Title Page

Abstract

Introduction

Conclusions

References

Tables

Figures

⏪

⏩

◀

▶

Back

Close

Full Screen / Esc

Printer-friendly Version

Interactive Discussion



supported by basal water pressure (Cuffey and Paterson, 2010). In models without an explicit hydrologic component, basal temperature is often used as a surrogate:

$$u_b = C(x, y)f(T_b)\tau_b^n \quad (2)$$

where T_b is the homologous basal temperature (relative to the pressure melt point), and f is zero for T_b below some threshold, usually a few degrees to tenths of a °C below freezing, ramping up to 1 at the melt point (e.g., Pattyn, 2010). In many large-scale models the same simple forms are also used for basal motion over deformable sediment, representing shearing within the sediment itself which is usually not modeled explicitly (cf. Howell and Siegert, 2000; Pollard and DeConto, 2003, 2007; Oerlemans and Nick, 2006). Values of $C(x, y)$ representing hard rock vs. deformable sediment vary by many orders of magnitude, roughly 10^{-10} to $10^{-5} \text{ m a}^{-1} \text{ Pa}^{-2}$, respectively for $n = 2$. In this paper we use essentially Eq. (2) with a weakly non-linear dependence on τ_b ($n = 2$). Other types of sliding laws are discussed briefly below.

The large-scale distributions of sediment vs. hard bed represented by $C(x, y)$, and hydrology represented by T_b or N , are probably the major sources of error in simulations of modern grounded Antarctic ice. Relevant data are sparse and/or indirect (e.g., Drewry, 1976; Studinger et al., 2001; Tulaczyk et al., 1998; Peters et al., 2006; Bingham and Siegert, 2009; Ferraccioli et al., 2009; Bell et al., 2011; Young et al., 2011). In comparison, other major factors are (i) better constrained by observations or experiment, such as surface and bed topography, surface velocity and mass balance, internal core temperature profiles and ice rheology, or (ii) arguably have lesser effects on large-scale ice geometry, such as non-uniform or anisotropic ice rheology, basal mass balance, geothermal heat flux, and neglect of longitudinal stresses in Shallow Ice Approximation (SIA) models. Although Heberler et al. (2008) found climate variations and other parameters to be as important as sliding in modeling Fennoscandian ice sheet geometry, their assumed range of sliding parameters was quite small compared to the potential sediment vs. hard-bed range. Our assertion is supported by Briggs et al.'s (2011) ensemble modeling of Antarctica, who found persistent errors that could not be reduced

Distribution of basal sliding coefficients under ice sheets

D. Pollard and
R. M. DeConto

Title Page

Abstract

Introduction

Conclusions

References

Tables

Figures

◀

▶

◀

▶

Back

Close

Full Screen / Esc

Printer-friendly Version

Interactive Discussion



by adjusting model parameters with $C(x, y)$ excluded. Whitehouse et al. (2012) found a similar strong sensitivity to basal sliding parameters in simulating the last Antarctic deglaciation.

Most previous paleoclimatic continental ice sheet models have widespread $O(100\text{'s m})$ errors in modern Antarctic surface elevations, with regional errors of 500 m or more (e.g., Ritz et al., 2001; Philippon et al., 2006; Pollard and DeConto, 2009; Whitehouse et al., 2012; Fig. 1a). In this paper we take the view that:

1. Such large errors are likely to undermine paleoclimatic and future modeling applications, and it is important to reduce them considerably. For instance, simulations of past and future stability of WAIS could be seriously astray if modern ice thicknesses in its major drainage basins are in error by 500 m or more.
2. Much of these errors are due to erroneous prescription of intrinsic bed properties $C(x, y)$, and not so much to errors in modeled basal temperatures or hydrology ($f(T_b)$ or N).

In support of the latter point, we note that most large-scale Antarctic models agree fairly well on the locations of basal freezing vs. melting areas, even using quite different maps of geothermal heat flux (e.g., Pattyn, 2010).

This paper describes a simple procedure to minimize errors in modern ice surface elevation by adjusting $C(x, y)$. The resulting $C(x, y)$ is mainly a model-derived estimate of the actual sediment vs. hard-rock distribution below Antarctica. The procedure tacitly assumes that all errors are due to unknown bed properties, and ignores any canceling errors due to imperfect basal temperatures and other model shortcomings. As ice models improve in the future and better observations of bed properties become available, canceling errors will hopefully be detectable, and model-derived $C(x, y)$ maps can be validated. For now, we suggest that the risk of canceling errors is the lesser of two evils, worth taking in order to eliminate $O(500\text{ m})$ errors in modern surface elevation.

The inverse method does not depend on the exact form of the sliding law, and in principle is applicable to any smoothly varying relation between u_b and τ_b , perhaps

Distribution of basal sliding coefficients under ice sheets

D. Pollard and
R. M. DeConto

Title Page

Abstract

Introduction

Conclusions

References

Tables

Figures

⏪

⏩

◀

▶

Back

Close

Full Screen / Esc

Printer-friendly Version

Interactive Discussion



even to multi-valued and bounded-drag forms (Schoof, 2005; Gagliardini et al., 2007; Pimentel et al., 2010) as long as intrinsic bed quantities can be adjusted to increase or decrease u_b for any given τ_b and hydrologic conditions. This is not the case for plastic rheology, with τ_b bounded by a given yield stress and no sliding for smaller τ_b (e.g., Bueler and Brown, 2009), which is not amenable to this inverse method.

The method also does not depend on model details outside of the sliding law, but the model does need to be run long enough for the procedure to converge, on the order of 200 000 yr for continental Antarctica. In principle it would be preferable to use a high-resolution model with full-Stokes or higher-order dynamics to fully capture ice streaming regions and grounding-line zones, but that is currently infeasible for 100 000 yr time scales. Here we use a coarse-grid model with a simpler hybrid treatment of longitudinal stresses, that allows long-term simulations while still producing reasonable streaming flow and grounding line migration (Pollard and DeConto, 2007, 2009, 2012; henceforth PD07, PD09, PD12).

2 Previous inverse modeling, contrast with current method, outline of paper

A number of previous studies have attempted to deduce basal stresses or sliding coefficients under modern ice sheets and glaciers, pioneered by MacAyeal (1992, 1993) and adapted for instance by Vieli and Payne (2003) and Joughin et al. (2004). Those studies were applied to limited regions and used relatively sophisticated control methods and the Shelfy Stream Approximation (SSA) equations appropriate for stretching flow. Recent approaches using similar variational or adjoint methods have been applied to the Pine Island/Thwaites Glacier areas (Joughin et al., 2009; Morlighem et al., 2010), and to continental Antarctica (Lingle et al., 2007; Larour et al., 2009). Also, Price et al. (2011) applied a simpler method to Greenland, and Le Brocq et al. (2009) linked a similar method with a basal hydrology model for WAIS. All these studies are based on fitting modeled ice velocities to observed surface or balance velocities, with ice thicknesses and elevations prescribed to modern observed; results for Antarctica are

Distribution of basal sliding coefficients under ice sheets

D. Pollard and
R. M. DeConto

Title Page

Abstract

Introduction

Conclusions

References

Tables

Figures

⏪

⏩

◀

▶

Back

Close

Full Screen / Esc

Printer-friendly Version

Interactive Discussion



briefly compared with ours in a later section. Other recent inverse methods (Arthern and Gudmundsson, 2010; Raymond Pralong and Gudmundsson, 2011; Jay-Allemand et al., 2011) are also based primarily on fitting modeled to observed ice velocities.

Here a much cruder algorithm is used, fitting to surface elevations, not velocities. The ice-sheet model is run forward in time, and the basal sliding coefficient C is periodically adjusted at each point according to the local elevation error (ignoring the fact that the dynamical equations are non-local). This is continued iteratively until the model surface elevations converge to the best fit with those observed. The advantages of this method are that (i) it does not rely on Lagrange-multiplier or adjoint versions of the model dynamics, and (ii) with the modification described in the next paragraph, it guarantees that the model will produce realistic modern ice thicknesses and elevations in subsequent runs with $C(x, y)$ prescribed from the inversion procedure. The procedure makes the implicit assumption that modern Antarctic elevations and temperatures are close to equilibrium with modern climate, i.e., unequibrated glacial-isostatic adjustments remaining from the last deglaciation are small. Given that assumption and others, in principle the method should yield the same results as the other velocity-fitting methods above, because of the close relationship between balance velocities, ice thicknesses and surface mass balance (see Sect. 8 and Appendices B and C).

The first inversion procedure described below ignores the influence of basal temperatures on sliding (by setting $f(T_b) = 1$ in Eq. 2), and is called the “first method” throughout the paper. However, the deduced distribution of $C(x, y)$ will always be somewhat at odds with the frozen areas implied by the model’s predicted basal temperatures. If the deduced $C(x, y)$ is prescribed in a subsequent normal (non-inverse) run, relatively large ice thickness and elevation errors will ensue. The problem is illustrated below, and is then solved by using a modified procedure called the “second method” below, where the model’s T_b is allowed to influence sliding during the inversion. The modified method yields a $C(x, y)$ pattern that, when prescribed in subsequent normal runs, maintains the same optimal fit to modern ice elevations and thicknesses. The potential for canceling errors is greater with the second method (and even the possibility of multiple

Distribution of basal sliding coefficients under ice sheets

D. Pollard and
R. M. DeConto

Title Page

Abstract

Introduction

Conclusions

References

Tables

Figures



Back

Close

Full Screen / Esc

Printer-friendly Version

Interactive Discussion

steady states with the same ice geometry produced by different T_b and C distributions), but as argued above, some amount of canceling errors may be preferable to serious inaccuracies in modern ice geometry.

Sections 3 and 4 outline the model formulation and describe the inversion procedure for $C(x, y)$. Section 5 presents results using the first inverse method with no influence of basal temperatures, and shows the expected degradation in subsequent normal integrations. Section 6 shows results using the second method with basal temperatures influencing sliding, and includes a sensitivity test to constrain the enhancement factor for internal ice deformation. Even though modern ice elevations are considerably improved at this point, significant small-scale errors persist over mountain ranges, notably the Transantarctics, where the model's frozen basal temperatures prevent sufficient flow across the range (cf. Kerr and Huybrechts, 1999). We hypothesize that this is due to flow in deep valleys not resolved by the model grid, and in Sect. 7 a new parameterization is applied based on sub-grid topographic relief that considerably improves the remaining ice elevation errors. Section 8 briefly compares our deduced distribution of $C(x, y)$ with earlier Antarctic inverse studies. The concluding Sect. 9 mentions some future directions including combining with statistical ensemble techniques. In appendices, we consider the effects of bedrock-model biases, compare surface velocities to observed (Rignot et al., 2011), and apply the method to deeper bed elevations in the Recovery Glacier basin proposed by Le Brocq et al. (2008).

3 Model outline

The ice sheet/shelf model used here is an updated version of that in PD07 and PD09. As described there, the ice dynamics is a heuristic combination of the scaled SIA and SSA equations for shearing and longitudinal stretching flow, respectively. A parameterization relating ice velocity across the grounding line to local ice thickness (Schoof, 2007) is imposed as an internal boundary-layer condition, so that grounding-line migration is simulated accurately without the need for very high $O(100\text{ m})$ resolution

Distribution of basal sliding coefficients under ice sheets

D. Pollard and
R. M. DeConto

Title Page

Abstract

Introduction

Conclusions

References

Tables

Figures



Back

Close

Full Screen / Esc

Printer-friendly Version

Interactive Discussion



Distribution of basal sliding coefficients under ice sheets

D. Pollard and
R. M. DeConto

Title Page

Abstract

Introduction

Conclusions

References

Tables

Figures

◀

▶

◀

▶

Back

Close

Full Screen / Esc

Printer-friendly Version

Interactive Discussion



(Schoof, 2007; Gladstone et al., 2010; Pattyn et al., 2012). A polar stereographic grid is used, with relatively coarse 40-km grid resolution that permits the numerous long runs needed for the paper; some tests at 20 km and 10 km are included later in Sect. 8 and the appendices, and show that the results are essentially unchanged at the higher resolutions, including in ice stream areas. All changes to the model since PD09 are described in PD12; changes that are particularly relevant for this paper are outlined here.

Surface mass balance is computed from observationally based datasets of modern climatological Antarctic precipitation and temperature (ALBMAP, Le Brocq et al., 2010; with accumulation from Van de Berg et al., 2006). Simple lapse-rate corrections are made for elevation differences from modern, and a basic Positive-Degree-Day scheme is used for melt (PD12). The bedrock model is as in PD07 and PD09, with local asthenospheric relaxation towards isostasy, and non-local lithospheric elastic deformation; the ice-free equilibrium bed topography is derived from modern observed (Le Brocq et al., 2010), isostatically rebounded with all ice removed. A simple two-value pattern of geothermal heat flux is prescribed with 54.6 mW m^{-2} under EAIS and 70 mW m^{-2} under WAIS. This seems preferable to choosing one or another of available geothermal datasets (Shapiro and Ritzwoller, 2004; Fox Maule et al., 2005) which differ considerably from each other on regional scales; as noted below, results are insensitive to the choice of dataset.

Changes to the model physics since PD09 include a new parameterization of oceanic melting below floating ice, a calving scheme, and sub-grid fractional area at the edges of floating ice shelves. Other changes include a wider basal temperature ramp from no sliding to full sliding (-3 to 0°C here, compared to -0.5 to 0°C in PD09), and linear rather than log-linear weighting of the no-sliding and full-sliding coefficients. That is, in this paper,

$$C' = (1 - r)C_{\text{froz}} + rC(x, y) \quad (3a)$$

whereas in PD09,

$$C' = C_{\text{froz}}^{1-r} C(x, y)^r \quad (3b)$$

In both cases, the weighting r is given by

$$r = \max[0, \min[1, (T_b - T_r)/(-T_r)]] \quad (4)$$

5 with the ramp-width temperature $T_r = -3^\circ\text{C}$ in this paper, and -0.5°C in PD09.

Here T_b is the basal homologous temperature, C' is the effective sliding coefficient used in the dynamics, $C(x, y)$ is the sliding coefficient for $T_b = 0^\circ\text{C}$, adjusted in the inversion procedure, and $C_{\text{froz}} = 10^{-20} \text{ m a}^{-1} \text{ Pa}^{-2}$ (which is small enough to prevent any discernible sliding, but is not exactly zero to avoid divide-by-zero exceptions in the numerics). It is unclear whether algebraic Eq. (3a) or geometric Eq. (3b) weighting of C_{froz} vs. $C(x, y)$, or something in between, is most realistic, and depends on how subgrid variations in basal stress are propagated upwards into the mean flow (Gudmunsson, 2003; Hindmarsh et al., 2006). Equation (3a) favors more sliding compared to Eq. (3b), and improves results where it is used in the later sections of this paper.

15 For many of the inverse runs in this paper, we are only concerned with grounded ice. Unless otherwise noted below, (i) grounding lines are constrained to modern observed locations, and (ii) ice fluxes across grounding lines and floating ice-shelf thicknesses are still predicted by the model, but a very crude “inversion” scheme is used for floating ice, whereby the sub-ice oceanic melt rate is adjusted locally at intervals so as to maintain floating thicknesses close to observed (similar to MacAyeal and Thomas, 2003; Joughin and Padman, 2003). This is not the focus of the paper, and is just an expedient to maintain realistic floating ice shelves while we concentrate on grounded ice.

Distribution of basal sliding coefficients under ice sheets

D. Pollard and
R. M. DeConto

Title Page

Abstract

Introduction

Conclusions

References

Tables

Figures

⏪

⏩

◀

▶

Back

Close

Full Screen / Esc

Printer-friendly Version

Interactive Discussion



4 Inversion procedure

The inversion procedure is very simple. The model (with grounding lines and floating ice constrained as described above) is run forward in time, starting from modern observed bed and ice surface elevations. As described in Sect. 3, the model is forced by constant observed climatology (Le Brocq et al., 2010), with lapse-rate corrections for changing surface elevations. Every 5000 yr, at each grid point with grounded ice, the local basal sliding coefficient $C(x, y)$ in Eq. (3a) is adjusted by a multiplicative factor:

$$C_{\text{new}}(x, y) = C(x, y)10^{\Delta z} \quad \text{where} \quad \Delta z = \max[-1.5, \min[1.5, (h_s - h_s^{\text{obs}})/500]] \quad (5)$$

where h_s is the current ice surface elevation and h_s^{obs} is that observed (m). The factor is constrained to be within the range $10^{-1.5}$ to $10^{1.5}$ (~ 0.03 to 30) to avoid overshoots and improve stability and convergence. Furthermore, $C(x, y)$ is not allowed to exceed $10^{-5} \text{ m a}^{-1} \text{ Pa}^{-2}$, representing the slipperiest deformable sediment. (If a limit of 10^{-6} is used, ice elevations in the Siple Coast region remain too high with insufficient sliding in streams; if 10^{-4} is used, the model is numerically unstable.)

In the first inverse method, basal sliding is unaffected by temperature (by setting $r = 1$ in Eq. 4). Adjusted $C(x, y)$ values are allowed to be as small as $10^{-20} \text{ m a}^{-1} \text{ Pa}^{-2}$; values below about 10^{-12} render basal sliding insignificant even for the highest shear stresses, so a lower limit of 10^{-20} allows the inversion scheme to find its own motionless “frozen” areas. In the modified second method presented below, basal sliding is affected by the model’s basal temperature T_b via Eqs. (3a) and (4), adjustments to $C(x, y)$ are only done for non-frozen points with $T_b > -3^\circ\text{C}$, and $C(x, y)$ is constrained to not fall below $10^{-10} \text{ m a}^{-1} \text{ Pa}^{-2}$ representing hard rough bedrock. (With a higher minimum, 10^{-9} say, basal flow is too rapid and the model EAIS is generally too thin.)

The interval of 5000 yr between adjustments, and the numbers in Eq. (5), are an efficient compromise that allows ice thicknesses and temperatures to respond partially to the iterative changes in $C(x, y)$, while keeping $C(x, y)$ on track towards the optimal distribution without overshoots. The simulations converge to a stable and essentially

Distribution of basal sliding coefficients under ice sheets

D. Pollard and
R. M. DeConto

Title Page

Abstract

Introduction

Conclusions

References

Tables

Figures

⏪

⏩

◀

▶

Back

Close

Full Screen / Esc

Printer-friendly Version

Interactive Discussion



invariant state after about 200 000 to 400 000 yr. Some slow, small regional-scale variations (few 10 m in ice elevation, few 10 000 yr timescale) continue indefinitely, but with insignificant effects on the deduced $C(x, y)$ values. An animation of the diminishing errors in a typical inversion run is provided as supplementary material, showing model-minus-observed surface elevation differences (m) every 5000 yr through the 400 000-yr run (resulting in Fig. 1d below).

As noted above, the point-by-point adjustment in Eq. (5) ignores the obvious fact that the ice dynamical equations are non-local and changes in $C(x, y)$ affect the ice distribution at other points. These non-local effects require more sophisticated control or adjoint treatments used in the studies mentioned above and in Sect. 8. But as shown below, the simple procedure does work pragmatically; i.e., it converges to a stable solution, and it reduces errors in ice elevations to very small values in most areas. Furthermore, with the modified second method, it fully takes into account the patterns of frozen vs. thawed beds predicted by the model's thermodynamics.

5 Results: first inversion method, without basal temperature influence

For purposes of comparison, the first column of panels in Fig. 1a–c shows results with a very simple two-value prescription of basal coefficients, i.e., a hard-rock value where ice-free isostatically rebounded modern bed elevations are above sea level, and a deformable-sediment value where they are below (Stuðinger et al., 2001; PD09; cf. Whitehouse et al., 2012). Here these values are 3×10^{-9} and $3 \times 10^{-8} \text{ ma}^{-1} \text{ Pa}^{-2}$, respectively, which produce more or less the smallest overall surface elevation errors, but much the same results are obtained with other pairs such as 10^{-10} and 10^{-5} . As shown in Fig. 1a, the departures from modern ice surface elevations are large, 500 m to 1000 m in places, and are typical of those in previous large-scale long-term Antarctic modeling mentioned above.

The second column of panels, Fig. 1d–f, shows results using the first inverse method described above, with no effect of temperatures on basal sliding, and with deduced

Distribution of basal sliding coefficients under ice sheets

D. Pollard and
R. M. DeConto

Title Page

Abstract

Introduction

Conclusions

References

Tables

Figures

⏪

⏩

◀

▶

Back

Close

Full Screen / Esc

Printer-friendly Version

Interactive Discussion



$C(x,y)$ values allowed to fall to $10^{-20} \text{ ma}^{-1} \text{ Pa}^{-2}$ mimicking “frozen” regions. There is a drastic reduction in surface elevation errors (Fig. 1d), which are less than 50 m in most areas. The deduced $C(x,y)$ map (Fig. 1e) has deformable-sediment values (10^{-5}) values in streaming ice regions such as the Siple coast and other marginal outlet channels, as expected. $C(x,y)$ values less than about 10^{-12} , shown as purple in Fig. 1e, allow essentially no basal motion and imply that the bed should be frozen there. Note that the Transantarctics and most of the Dronning Maud Land mountains do not have these low values, and have high sediment-like values in some channels, i.e., the inversion procedure requires that ice slides easily over these mountain ranges (at least at 40 km resolution, discussed further below). The purple regions in Fig. 1e can be compared with the frozen-bed areas in Fig. 1f ($T_b < -3^\circ\text{C}$) predicted by the model thermodynamics. Although similar on the broadest scales, there are substantial regional differences, in particular over the Transantarctics which have quite high sliding coefficients in Fig. 1e but frozen basal temperatures in Fig. 1f. One can anticipate that surface elevation errors will worsen in these regions if the model is run in normal (non-inverse) mode with $C(x,y)$ prescribed from Fig. 1e, and with T_b allowed to influence sliding in Eq. (4).

The third column in Fig. 1 shows just that. The deduced basal coefficient map in Fig. 1e is first filled by replacing patches of $C < 10^{-10}$ with nearest-neighbor values $\geq 10^{-10}$. The resulting $C(x,y)$ map (Fig. 1h) is prescribed in a normal model run in which basal sliding is zero if the homologous basal temperature T_b is -3°C or below (Eqs. 3a and 4), and results are shown in Fig. 1g,i. As expected, errors in ice surface elevations in Fig. 1g are much worse than in Fig. 1d. For instance, over the Transantarctics the model predicts a frozen base and no sliding, and ice surface elevations are ~ 500 m or more too high.

To improve matters, one strategy would be to attempt to tune the model’s thermodynamics to replicate the implied frozen regions of the inversion procedure (purple patches in Fig. 1e), perhaps by including new hydrologic processes (Bell et al., 2011). Although that might turn out to be a valid future path, we note that the model’s basal

Distribution of basal sliding coefficients under ice sheets

D. Pollard and
R. M. DeConto

Title Page

Abstract

Introduction

Conclusions

References

Tables

Figures

⏪

⏩

◀

▶

Back

Close

Full Screen / Esc

Printer-friendly Version

Interactive Discussion



temperature map (T_b) is relatively insensitive to most “easy” changes, such as alternate geothermal heat flux maps (Shapiro and Ritzwoller, 2004; Fox Maule et al., 2005) and different parameterizations for ice conductivity and specific heat. Furthermore, the model’s T_b pattern is much the same in all cases here (bottom panels of most figures), and agrees quite closely with many other Antarctic models (e.g., Pattyn, 2010): frozen on buried mountain ranges and slow-flowing marginal flanks where thinner ice provides little insulation from the cold surface, and melting elsewhere, especially in fast-flowing streams and focused outlet channels. So for now we do not attempt to significantly change T_b , and choose an alternate strategy as described in the next section.

6 Results: second inversion method, with basal temperature influence

The mismatch between the inverse-procedure’s basal coefficients C and the model’s basal temperature T_b can be eliminated by

1. allowing T_b to influence sliding during the inversion integration, and
2. constraining C to remain between hard rock and sediment values (10^{-10} and $10^{-5} \text{ ma}^{-1} \text{ Pa}^{-2}$), and only adjusting it (Eq. 5) if the base is not completely frozen ($T_b > -3^\circ\text{C}$).

As discussed above, this increases the likelihood of canceling errors, but it does keep ice surface elevation errors small in subsequent non-inverse runs. In fact, there is no change at all in the modeled ice state between the end of this inverse method and a subsequent run with $C(x, y)$ prescribed from the inversion.

The viability of this second method is shown in the third column of Fig. 2 (panels g–i; also shown in Fig. 3a–c), where surface elevation errors are very small (few 10 m) over most non-mountainous regions, compared to Fig. 1g. The next section will address the remaining errors over mountain ranges. The rest of Fig. 2 is a tuning exercise to crudely constrain the internal-flow enhancement factor E , that multiplies all strain rates

Distribution of basal sliding coefficients under ice sheets

D. Pollard and
R. M. DeConto

Title Page

Abstract

Introduction

Conclusions

References

Tables

Figures



Back

Close

Full Screen / Esc

Printer-friendly Version

Interactive Discussion



$\partial u / \partial z$ in Glen's law within the SIA model (enhancement factors are commonly used in ice sheet models to improve large-scale results; e.g., Ritz et al., 2001).

Each column of panels in Fig. 2 shows results for a given E , from $E = 0.1$ to $E = 8$. With much smaller E (0.1 to 0.5, first two columns), there is very little internal flow, and the inversion procedure attempts to compensate by assigning higher values of $C(x, y)$ everywhere – but it cannot where the bed is frozen, so ice elevations in some regions become too high. As mentioned above, the third column with $E = 1$ gives the best overall results. For larger values of E (2 to 8, last three columns), there is too much internal flow, often exceeding the balance velocities implied by the surface mass balance. The inversion procedure cannot completely compensate even by setting $C(x, y)$ to the smallest (hard-rock, 10^{-10}) value, and surface elevations are generally much too low. We conclude that $E = 1$ is the most realistic internal-flow enhancement factor for this model, and have used that value for all other simulations in this paper.

Rignot et al. (2011) performed a similar estimate of the deformational factor for modern Antarctica, by fitting to observed surface velocities in divide regions where internal deformation is expected to dominate ice motion. As they discuss, most internal deformation occurs near the base in ice within a few °C of the melt point. Their deduced creep parameter value of $9 \times 10^{-25} \text{ s}^{-1} \text{ Pa}^{-3}$ agrees well with ours, which for $E = 1$ and homologous temperature of -5°C (mentioned in their Supplement) is $14.6 \times 10^{-25} \text{ s}^{-1} \text{ Pa}^{-3}$ (PD12).

One could conceivably attempt to further refine the model's internal flow physics, perhaps with spatially varying E or anisotropic rheology (e.g., Wang and Warner, 1999; Graverson et al., 2011). But these refinements would likely be beyond the scope of the present approach. As discussed in the introduction, one assumption of this paper is that large-scale ice elevation errors caused by deficiencies in internal flow are minor compared to those caused by unrealistic bed sliding.

Distribution of basal sliding coefficients under ice sheets

D. Pollard and
R. M. DeConto

[Title Page](#)[Abstract](#)[Introduction](#)[Conclusions](#)[References](#)[Tables](#)[Figures](#)[⏪](#)[⏩](#)[◀](#)[▶](#)[Back](#)[Close](#)[Full Screen / Esc](#)[Printer-friendly Version](#)[Interactive Discussion](#)

7 Results: second inversion method, with basal temperature and topographic influence

As noted above, the results of the second inverse method (with basal temperature influence) are identical to those when the deduced basal coefficient map $C(x, y)$ is prescribed in a non-inverse run, which is definitely not the case with the first inverse method (without basal temperature influence). The second method's surface elevation errors (Fig. 3a) are much smaller than those using the first method's $C(x, y)$ in a non-inverse run, as shown in Fig. 1g. However, ice elevations are still too high by several hundred meters over most of the Transantarctics and some other mountain ranges (Fig. 3a). There the model's basal temperatures are uniformly frozen, and the inversion procedure cannot compensate for the hindrance to cross-range flow. To some extent, frozen basal temperatures are expected over mountain ranges, because the thinner ice provides relatively little insulation from cold surface temperatures (Pattyn, 2010). However, there may still be significant basal sliding in deep and warmer valleys, not resolved by the coarse grids used here. We attempt to parameterize this sub-grid process by modifying the width of the basal-temperature ramp T_r in Eq. (4) as a function of sub-grid topographic variations. The constant value $T_r = -3^\circ\text{C}$ used above is replaced by

$$T_r = -3 - 500 \max[\text{SA} - 0.02, 0] - 0.05 \max[h_b^{\text{eq}} - 1700, 0] \quad (6)$$

where SA is the mean sub-grid slope amplitude computed by averaging the bed slopes in the 5-km ALBMAP dataset (Le Brocq et al., 2010) within each model grid box. h_b^{eq} is the ice-free isostatically rebounded (and 9-point smoothed) bed elevation on the coarse model grid, discussed below. SA was also used by Marshall et al. (1996) in another context. Whitehouse et al. (2012) apply a similar increase in sliding coefficient over mountainous terrain, for much the same reasons.

SA is typically ~ 0.02 or less in plains, and ~ 0.03 to 0.05 or more in mountain ranges where T_r can typically be $\sim -15^\circ\text{C}$ or colder. However, around the Gamburtsevs and

TCO

6, 1405–1444, 2012

Distribution of basal sliding coefficients under ice sheets

D. Pollard and
R. M. DeConto

Title Page

Abstract

Introduction

Conclusions

References

Tables

Figures

◀

▶

◀

▶

Back

Close

Full Screen / Esc

Printer-friendly Version

Interactive Discussion



Distribution of basal sliding coefficients under ice sheets

D. Pollard and
R. M. DeConto

Title Page

Abstract

Introduction

Conclusions

References

Tables

Figures

⏪

⏩

◀

▶

Back

Close

Full Screen / Esc

Printer-friendly Version

Interactive Discussion

also the extreme Southern Transantarctics (~ 120 to 180° W), SA seems to be anomalously low, presumably due to the sparsity of BEDMAP data lines (Lythe et al., 2001). Hence the second term in Eq. (6) uses the grid-scale elevation h_b^{eq} as a surrogate. h_b^{eq} is less than 1700 m nearly everywhere except over those two regions, where it is typically ~ 2000 m or more, so again T_r can typically be $\sim -15^\circ\text{C}$ or colder. The use of h_b^{eq} is based only on the assumption that very high regions also have high sub-grid variability; future improvements in topographic coverage will probably allow just the first term in Eq. (6) to be used (Bo et al., 2009; Bell et al., 2011; Young et al., 2011).

Using Eq. (6), the inversion procedure with T_b influencing sliding produces the smallest elevation errors of all simulations, shown in Fig. 3d–f (second column). Now, more basal sliding over mountain ranges occurs despite frozen basal temperatures, reducing too-high surface errors. Remaining elevation errors in Fig. 3d are mostly < 50 m, except in a few small patches over mountains. We emphasize again that this realism is retained in non-inverse runs with $C(x, y)$ prescribed from the second inversion procedure, to be compared with the much poorer results in non-inverse runs with $C(x, y)$ prescribed from the first inversion procedure that ignores basal temperature effects (Fig. 1g).

In all simulations to this point, the focus has been on replicating modern Antarctic grounded ice, so grounding lines have been fixed at their present positions, and floating ice thicknesses have been artificially constrained to remain close to observed. Fig. 3g,h (third column) shows that when all these constraints are relaxed and the complete ice sheet-shelf model is integrated forward with $C(x, y)$ prescribed from Fig. 3e, there is only a little degradation of ice elevations, and modern errors remain less than ~ 50 m nearly everywhere. The Filchner-Ronne grounding line recedes slightly too much in the Eastern Weddell Sea, causing negative ice elevation errors there (Fig. 3g); also, the model fails to simulate the George VI Sound and ice shelf between Alexander Island and the Western Peninsula, causing positive elevation errors. But overall, the unconstrained model, with prescribed basal sliding coefficients $C(x, y)$ from the second

inverse method and including the topographic influence in Eq. (6), produces a modern ice distribution very close to observed.

8 Finer resolution, and comparison with previous Antarctic inverse modeling

As described in Sect. 2, a number of previous studies have deduced maps of basal stress or sliding coefficients under modern Antarctica. Most have used the SSA (Shelfy Stream Approximation) or higher-order equations, and relatively sophisticated control or adjoint methods to more rigorously account for the non-local nature of the dynamics. Published Antarctic studies have targeted limited regions at higher resolutions, rather than all Antarctica at 40 km as in this study. In contrast to the present method, the above studies have fitted to observed velocities with ice thicknesses prescribed; however, in principle the resulting basal maps should be similar due to the interdependence of equilibrium velocities, ice thicknesses and surface mass balance.

To better compare with earlier studies, and also to test for grid-size dependence within our model, Fig. 4 show results at somewhat higher resolutions of 20 and 10 km. Compared with the corresponding 40-km results in Fig. 3d–i, some finer details emerge, but the large-scale pattern of basal coefficients and the amplitude of surface elevation errors remain essentially the same at the higher resolutions. This is true even for ice streaming regions such as the Siple coast, where 40-km resolution is not expected to resolve individual ice streams. The proto-streaming in the 40-km grid requires the same sliding coefficients as in the finer grids to produce the same regional ice thicknesses.

Most previous inverse studies have deduced basal stresses or used different sliding laws than ours, so comparisons with our basal coefficient maps can only be qualitative. Joughin et al. (2009) and Morlighem et al. (2010) deduced basal stresses in the Thwaites (TG) and Pine Island Glacier (PIG) areas. Comparing their maps with our $C(x, y)$ pattern at 10-km resolution in Fig. 4h, there are some encouraging zeroth-order points of agreement: (i) immediately upstream of the PIG grounding line, there is

Distribution of basal sliding coefficients under ice sheets

D. Pollard and
R. M. DeConto

Title Page

Abstract

Introduction

Conclusions

References

Tables

Figures



Back

Close

Full Screen / Esc

Printer-friendly Version

Interactive Discussion



a O (10 km) strip with higher basal stress and lower C values, then a large O (100 km)-long broadening zone with low stresses and high C values. (ii) ~ 100 to 200 km upstream (southward) from the TG grounding line, there are transverse strips of alternating high/low stresses and high/low C values, similar to more numerous strips in Joughin et al. (2009).

On continental scales, there is some agreement between Fig. 4e and all-Antarctic maps deduced using other models and sliding laws (Lingle et al., 2007; Larour et al., 2009); i.e., generally smaller sliding coefficients in the continental interiors, and larger values in marginal areas of streaming flow (e.g., Siple coast) and major outlet channels (e.g., Recovery Glacier). Optimistically, this agreement is due to the models all more or less capturing the real large-scale distribution of sediment vs. hard rock. However, at regional and local scales there is only sporadic agreement between Fig. 4e and the other model maps.

9 Summary and conclusions

A simple inverse method of adjusting basal sliding coefficients to minimize modern ice surface elevation errors (Eq. 5) drastically reduces these errors in our continental-scale Antarctic model. Unlike the more sophisticated control or adjoint methods used in previous inverse studies, the method is local and ignores the spatial connectivity of ice dynamics. With basal temperatures included in the sliding parameterization during the inversion procedure, realistic ice elevations are maintained in subsequent forward calculations with prescribed sliding coefficients.

Clearly there is a danger of canceling errors; i.e., the deduced sliding coefficients $C(x, y)$ may not be real, but instead might be compensating for errors in the model physics or other input datasets. Our $C(x, y)$ probably do represent a combination of (i) model errors, (ii) omitted physical variables affecting sliding such as overburden pressure or hydrologic regime, and (iii) all intrinsic bed properties that affect sliding, not just sediment vs. hard rock but also small-scale roughness. In the future it may

Distribution of basal sliding coefficients under ice sheets

D. Pollard and
R. M. DeConto

Title Page

Abstract

Introduction

Conclusions

References

Tables

Figures

⏪

⏩

◀

▶

Back

Close

Full Screen / Esc

Printer-friendly Version

Interactive Discussion



become possible to sort this out with better (higher-order, higher-resolution) models and new improved datasets, and achieve convergence between models and data on real Antarctic bed conditions. For now, we suggest that the danger of canceling errors is preferable to using ice models with very large ($>\sim 500$ m) elevation biases to study important problems such as past and future stability of WAIS.

In conjunction with the basal inverse method, we also coarsely constrained the internal-flow enhancement factor E , by finding the bounds outside of which the basal inversion cannot maintain a realistic ice distribution (Fig. 2). This provides reasonable uniform constraints on E , but as discussed above, further refinement of internal-flow physics involving anisotropic rheology or spatially varying E is beyond the scope of the methods used here.

To further reduce small patches of surface elevation errors ($O(100$'s m)) over mountain ranges such as the Transantarctics, the influence of basal temperature on sliding had to be modified to include sub-grid topographic variations (Eq. 6). Without this, frozen basal temperatures hinder sliding too much across major mountain ranges, causing local ice to be too thick. This parameterization of basal flow in deep sub-grid valleys can be tested in future work by higher-resolution models (cf. Egholm et al., 2011).

Directions for future work include combining the basal inverse method with statistical ensemble techniques involving other model parameters (Hebeler et al., 2008; Stone et al., 2010; Applegate et al., 2011; Briggs et al., 2011; Tarasov et al., 2012); this could test our assertion that basal properties are one of the largest sources of uncertainty in ice-sheet modeling. The inverse method could also be combined with basal hydrologic modeling following Le Brocq et al. (2009). The assumption of modern quasi-equilibrium, especially for internal and basal temperatures, can be tested by integrating through the last few 10 000 yr (although we have previously found that modern ice thicknesses and grounding line locations are much the same in modern equilibrated vs. transient runs, not shown). Whitehouse et al. (2012) have recently developed a deglacial model of Antarctica from 20 ka to the present, and performed an

Distribution of basal sliding coefficients under ice sheets

D. Pollard and
R. M. DeConto

[Title Page](#)[Abstract](#)[Introduction](#)[Conclusions](#)[References](#)[Tables](#)[Figures](#)[⏪](#)[⏩](#)[◀](#)[▶](#)[Back](#)[Close](#)[Full Screen / Esc](#)[Printer-friendly Version](#)[Interactive Discussion](#)

low; this is likely caused by isostatic depression under too thick ice over local mountains (Fig. 4d). It seems likely that such small bedrock errors have had a very minor effect on the inverse results presented above. We tested this explicitly in one case, repeating the inverse run in Fig. 4d–f except with bedrock physics switched off so that bed elevations remain exactly at modern values. The results for surface elevations, basal coefficients and temperatures were essentially unchanged from those in Fig. 4d–f. Note, however, that bed elevation errors of this order might be significant for other purposes, for instance in comparing with Relative Sea Level records. Also, note that the closeness of the agreement with observed modern bed elevations is somewhat fortuitous, because the model has not taken transient residuals from the last deglaciation into account (see Appendix B, Fig. B1b).

Appendix B

Equilibrated versus transient modern state

In the inverse procedure, the model is forced with invariant modern climate, but its ice surface results are compared with modern observations. Any unequilibrated Glacial-Isostatic Adjustments (GIA) remaining from the last deglaciation are not accounted for in the model, and are implicitly assumed to be small. This mainly concerns ice mass inertia, lagged isostatic bed response, and ice temperatures through their effect on rheology and sliding. In future work we plan to combine the inverse method with transient runs through the last deglaciation, comparing in depth with relevant data (Sect. 9; cf. Briggs et al., 2011; Whitehouse et al., 2012). For now, we can estimate the magnitude of this bias in the current results, by comparing the model's equilibrated modern state with that at the end of a transient run through the last several 10 000's years. Results are shown in Fig. B1, where the transient simulation was run from 80 ka to the present, with paleoclimatic air temperatures, precipitation, oceanic melt rates and sea level parameterized as in PD12 (similarly to PD09).

Distribution of basal sliding coefficients under ice sheets

D. Pollard and
R. M. DeConto

Title Page

Abstract

Introduction

Conclusions

References

Tables

Figures



Back

Close

Full Screen / Esc

Printer-friendly Version

Interactive Discussion



Distribution of basal sliding coefficients under ice sheets

D. Pollard and
R. M. DeConto

Title Page

Abstract

Introduction

Conclusions

References

Tables

Figures

⏪

⏩

◀

▶

Back

Close

Full Screen / Esc

Printer-friendly Version

Interactive Discussion

As shown in Fig. B1a, surface elevations on the East Antarctic central plateau continue to increase by ~ 20 to 50 m after 0 ka, if the model is allowed to equilibrate to modern forcing, presumably due to the increase in snowfall rates over the last deglaciation. Conversely, surface elevations fall in many regions closer to the East Antarctic coast, generally coinciding with high bedrock topography and frozen basal temperatures. This may be due to continued warming of internal ice temperatures, lower ice viscosities and greater SIA shear flow. The marked increase in elevations over the Siple Coast is due to the model grounding line re-advancing slightly after 0 ka (seen in Fig. B1c vs. d), due to continuing bedrock rebound after the last deglaciation which causes grounding-line depths to shoal slightly. Changes in bed elevations (Fig. B1b) generally mirror the ice surface changes (smaller, with opposite sign, as expected due to isostatic relaxation), at least in East Antarctica. There is very little change in the frozen vs. melting pattern of basal temperatures (Fig. B1c–d).

We plan to assess all these effects as part of further transient modeling of the last deglaciation (Sect. 9). Here, we note that the differences in ice surface elevations (Fig. B1a) are on the order of 20 to 50 m in most areas. These are on the same order as the residual large-scale elevation errors vs. observed achieved by the inverse method (Figs. 3 and 4, top rows), and are much smaller than the many 100's m elevation biases with simple $C(x, y)$ distributions that the method has already corrected for (Fig. 1a). Therefore, when the inversion method is extended in future work to properly account for transient effects, we anticipate that the deduced $C(x, y)$ patterns will change only slightly in order to adjust for the elevation differences in Fig. B1a, and the overall $C(x, y)$ results presented above will remain very much the same.

Appendix C

Comparison with observed velocities

As mentioned above, in contrast to previous basal inversion modeling, the current method is based on fitting to observed ice elevations, not velocities. Nevertheless, our surface velocities should agree with those observed, given a number of conditions:

- i. the modern surface mass balance dataset used here is correct (Van de Berg, 2006; in ALBMAP; Le Brocq et al., 2010)
- ii. any basal mass balance (melting, refreezing) errors in the model are negligible,
- iii. the model ice thicknesses are correct,
- iv. the model's split between surface and depth-average velocities is correct,
- v. both the model and real modern Antarctic ice sheets are close to equilibrium (see Appendix B).

A new all-Antarctic dataset of surface velocities (Rignot et al., 2011) provides the opportunity to test this, as shown in Fig. C1 where the dataset (900 m spacing) has been regrided by simple area-averaging to the model's 20 km grid. Quantitative comparison is hindered by the fine scale and sharp gradients of many features in the dataset such as numerous outlet glaciers around the coast, many of which are barely resolved by the model and may be slightly displaced to one side or the other. Model speeds in the flanks around most coastlines are generally too fast, both in outlet glaciers and in the slower flow between them. The model's marginal ice thicknesses are generally close to observed (Fig. 4d), so the discrepancy might be caused by too much snowfall near the coasts, or too much internal deformation compared to sliding. The biggest single velocity error in Fig. C1c is due to the Kamb Ice Stream (Ice Stream C) on the Siple Coast, which stagnated about 150 yr ago (Hulbe and Fahnestock, 2007), but in the model is flowing at velocities comparable to the other active Ross ice streams.

Distribution of basal sliding coefficients under ice sheets

D. Pollard and
R. M. DeConto

Title Page

Abstract

Introduction

Conclusions

References

Tables

Figures



Back

Close

Full Screen / Esc

Printer-friendly Version

Interactive Discussion



Appendix D

Recovery Glacier basin topography

5 Recently Le Brocq et al. (2008) suggested, based on observed ice surface curvatures, that much of the bed in the catchment of Recovery Glacier (a major system flowing into the Filchner Ice Shelf) may be much deeper than previously thought, up to ~ 1500 m below sea level and layered with deformable sediments (Fig. D1). Le Brocq et al. (2011) found that the deeper topography improved modern surface elevations and velocities in their regional ice sheet simulations (their Fig. 3). By applying the inversion procedure with both the standard and deeper topographies (both available in ALBMAP; Le Brocq et al., 2010), we can test if one or the other is more viable from the point of view of inverse-fitting to ice surface elevations. Figure D2 shows results using the second inverse method with basal temperature and sub-grid topography influencing sliding, in a nested domain with 10 km resolution.

15 As might be expected, the deeper topography requires slower sliding velocities to compensate for the thicker ice (Fig. D2d,h), which is accomplished by the inversion procedure deducing somewhat less deformable sediment in the deeper Recovery and Slessor glacier channels (Fig. D2b,f). The surface elevation errors are generally slightly less with the “standard” topography, although both have errors of several hundred meters (of opposite sign) on the ridge between Slessor and Recovery glaciers (Fig. D2a, e). Some of the elevation errors coincide with patches of frozen vs. melting bed (Fig. D2c, g), suggesting that the model’s thermodynamics and parameterized effects of basal temperature and sliding might be at fault; however, much the same results are obtained with the first inverse method (no effect of basal temperatures on sliding as in Fig. 1d–f; not shown); i.e., both cases yielding similar surface elevation errors, slightly smaller in the standard topography case. On the other hand, the deeper topography produces a somewhat more realistic surface velocity map (Fig. D2, bottom row).

Distribution of basal sliding coefficients under ice sheets

D. Pollard and
R. M. DeConto

Title Page

Abstract

Introduction

Conclusions

References

Tables

Figures

◀

▶

◀

▶

Back

Close

Full Screen / Esc

Printer-friendly Version

Interactive Discussion



Given these mixed results, we suggest that the methods used here cannot definitely distinguish between the two topographies.

Supplementary material related to this article is available online at:
<http://www.the-cryosphere-discuss.net/6/1405/2012/tcd-6-1405-2012-supplement.zip>.

Acknowledgements. This research was funded by the US National Science Foundation under awards ANT 0424589, 1043018, 25-0550-0001, and OCE-1202632.

References

- Applegate, P. J., Kirchner, N., Stone, E. J., Keller, K., and Greve, R.: Preliminary assessment of model parametric uncertainty in projections of Greenland Ice Sheet behavior, *The Cryosphere Discuss.*, 5, 3175–3205, doi:10.5194/tcd-5-3175-2011, 2011.
- Arthern, R. J. and Gudmundsson, G. H.: Initialization of ice-sheet forecasts viewed as an inverse Robin problem, *J. Glaciol.*, 56, 527–533, 2010.
- Bassett, S. J., Milne G. A., Bentley M. J., and Huybrechts, P.: 2007. Modelling Antarctic sea-level data to explore the possibility of a dominant Antarctic contribution to meltwater pulse 1 A, *Quaternary Sci. Rev.*, 26, 2113–2127, 2007.
- Bell, R. E., Ferraccioli, F., Creyts, T. T., Braaten, D., Corr, H., Das, I., Damaske, D., Frearson, N., Jordan, T., Rose, K., Studinger, M., and Wolovick, M.: Widespread persistent thickening of the East Antarctic ice sheet by freezing from the base, *Science*, 331, 1592–1595, 2011.
- Bo, S., Siegert, M. J., Mudd, S. M., Sugden, D., Fujita, S., Xiangbin, C., Yunyun, J., Xueyuan T., and Yuansheng, L.: The Gamburtsev mountains and the origin and early evolution of the Antarctic ice sheet, *Nature*, 459, 690–693, 2009.
- Bingham, R. G. and Siegert, M. J.: Quantifying subglacial bed roughness in Antarctica: implications for ice-sheet dynamics and history, *Quaternary Sci. Rev.*, 28, 223–236, 2009.
- Briggs, R., Pollard, D., and Tarasov, L.: Past evolution of the Antarctic ice sheet: a Bayesian calibrated 3D glacial system modeling study, in: Programme and Abstracts, 11th International

Distribution of basal sliding coefficients under ice sheets

D. Pollard and
R. M. DeConto

Title Page

Abstract

Introduction

Conclusions

References

Tables

Figures

⏪

⏩

◀

▶

Back

Close

Full Screen / Esc

Printer-friendly Version

Interactive Discussion



Distribution of basal sliding coefficients under ice sheetsD. Pollard and
R. M. DeConto

Title Page

Abstract

Introduction

Conclusions

References

Tables

Figures

◀

▶

◀

▶

Back

Close

Full Screen / Esc

Printer-friendly Version

Interactive Discussion

Symposium on Antarctic Earth Sciences, 10–16 July 2011, Edinburgh, Scotland, 246 pp., Abstract PS19.9, 2011.

Bueler, E. and Brown, J.: Shallow shelf approximation as a “sliding law” in a thermomechanically coupled ice sheet model, *J. Geophys. Res.*, 114, F03008, doi:10.1029/2008JF001179, 2009.

5 Cuffey, K. M. and Paterson, W. S. B.: *The Physics of Glaciers*, 4th edn., Academic Press, Amsterdam, 704 pp., 2010.

Dowdeswell, J. A. and Siegert, M. J.: Ice-sheet numerical modeling and marine geophysical measurements of glacier-derived sedimentation on the Eurasian Arctic continental margins, *Geol. Soc. Am. Bull.*, 111, 1080–1097, 1999.

10 Drewry, D. J.: Sedimentary basins of the East Antarctic craton from geophysical evidence, *Tectonophysics*, 36, 301–314, 1976.

Egholm, D. L., Knudsen, M. F., Clark C. D., and Lesemann, J. E.: Modeling the flow of glaciers in steep terrains: the integrated second-order shallow ice approximation (iSOSIA), *J. Geophys. Res.*, 116, F02012, doi:10.1029/2010JF001900, 2011.

15 Ferraccioli, F., Armadillo, E., Jordan, T., Bozzo, E., and Corr, H.: Aeromagnetic exploration over the East Antarctic ice sheet: a new view of the Wilkes Subglacial Basin, *Tectonophysics*, 478, 62–77, 2009.

Fox Maule, C., Purucker, M. E., Olsen, N., and Mosegaard, K.: Heat flux anomalies in Antarctica revealed by satellite magnetic data, *Science*, 309, 464–467, 2005.

20 Gagliardini, O., Cohen, D., Raback, P., and Zwinger, T.: Finite-element modeling of subglacial cavities and related friction law, *J. Geophys. Res.*, 112, F02027, doi:10.1029/2006JF000576, 2007.

Gladstone, R. M., Lee, V., Vieli, A., and Payne, A. J.: Grounding line migration in an adaptive mesh ice sheet model, *J. Geophys. Res.*, 115, F04014, doi:10.1029/2009JF001615, 2010.

25 Gomez, N., Mitrovica, J. X., Tamisiea, M. E., and Clark, P. U.: A new projection of sea level change in response to collapse of marine sectors of the Antarctic ice sheet, *Geophys. J. Int.*, 180, 623–634, 2010.

Graversen, R. G., Drijfhout, S., Hazeleger, W., van de Wal, R., Bintanja R., and Helsen, M.: Greenland’s contribution to global sea-level rise by the end of the 21st century, *Clim. Dyn.*, 37, 1427–1442, 2011.

30 Gudmundsson, G. H.: Transmission of basal variability to a glacier surface, *J. Geophys. Res.*, 108, 2253, doi:10.1029/2002JB002107, 2003.

Distribution of basal sliding coefficients under ice sheets

D. Pollard and
R. M. DeConto[Title Page](#)[Abstract](#)[Introduction](#)[Conclusions](#)[References](#)[Tables](#)[Figures](#)[⏪](#)[⏩](#)[◀](#)[▶](#)[Back](#)[Close](#)[Full Screen / Esc](#)[Printer-friendly Version](#)[Interactive Discussion](#)

- Hebeler, F., Purves, R. S., and Jamieson, S. S. R.: The impact of parametric uncertainty and topographic error in ice-sheet modeling, *J. Glaciol.*, 54, 899–919, 2008.
- Hindmarsh, R. C. A., Leysinger Vieli, G. J.-M. C., Raymond M. J., and Gudmundsson, G. H.: Draping or overriding: the effect of horizontal stress gradients on internal layer architecture in ice sheets, *J. Geophys. Res.*, 111, F02018, doi:10.1029/2005JF000309, 2006.
- Howell, D. and Siegert, M. J.: Intercomparison of subglacial sediment-deformation models: application to the late Weischelian Western Barents margin, *Ann. Glaciol.*, 30, 187–196, 2000.
- Hulbe, C. and Fahnestock, M.: Century-scale discharge stagnation and reactivation of the Ross ice streams, West Antarctica, *J. Geophys. Res.*, 112, F03S27, doi:10.1029/2006JF000603, 2007.
- Ivins, E. R. and James, T. S.: Antarctic glacial isostatic adjustment: a new assessment. *Antarc. Sci.*, 17, 541–553, 2005.
- Jamieson, S. S. R. and Sugden, D. E.: Landscape evolution of Antarctica, in: *Antarctica: a Keynote to a Changing World*, Proceedings of the 10th International Symposium on Antarctic Earth Science, Cooper, A. K. (eds.), National Academics Press, Washington DC, 39–54 pp., 2008.
- Jamieson, S. S. R., Sugden, D. E., and Hulton, N. R. J.: The evolution of the subglacial landscape of Antarctica, *Earth Plan. Sci. Lett.*, 293, 1–27, 2010.
- Jay-Allemand, M., Gillet-Chaulet, F., Gagliardini, O., and Nodet, M.: Investigating changes in basal conditions of Variegated Glacier prior to and during its 1982–1983 surge, *The Cryosphere*, 5, 659–672, doi:10.5194/tc-5-659-2011, 2011.
- Joughin, I. and Padman, L.: Melting and freezing beneath Filchner-Ronne ice shelf, Antarctica, *Geophys. Res. Lett.*, 30, 1477, doi:10.1029/2003GL016941, 2003.
- Joughin, I., MacAyeal, D. R., and Tulaczyk, S.: Basal shear stress of the Ross ice streams from control method inversions, *J. Geophys. Res.*, 109, B09405, doi:10.1029/2003JB002960, 2004.
- Joughin, I., Tulaczyk, S., Bamber, J. L., Blankenship, D., Holt, J. W., Scambos T., and Vaughan, D. G.: Basal conditions for Pine Island and Thwaites Glaciers, West Antarctica, determined using satellite and airborne data, *J. Glaciol.*, 55, 245–257, 2009.
- Kerr, A. and Huybrechts, P.: The response of the East Antarctic ice-sheet to the evolving tectonic configuration of the Transantarctic mountains, *Glob. Plan. Change*, 23, 213–229, 1999.

Distribution of basal sliding coefficients under ice sheets

D. Pollard and
R. M. DeConto

Title Page

Abstract

Introduction

Conclusions

References

Tables

Figures

◀

▶

◀

▶

Back

Close

Full Screen / Esc

Printer-friendly Version

Interactive Discussion



- Larour, E., Rignot, E., Seroussi, H., Morlighem, M., Menemenlis, D., and Schodlock, M.: ISSM: Ice Sheet System Model – large scale, high resolution modeling of ice-sheet flow, with data assimilation coupled with an ocean model, JPL PARCA meeting, Seattle, Washington, USA, 30 September–1 October, 2009, available online: <http://issm.jpl.nasa.gov/files/issm/LarourParca09.pdf>, 2009.
- Le Brocq, A. M., Hubbard, A., Bentley, M. J., and Bamber, J. L.: Subglacial topography inferred from ice surface terrain analysis reveals a large un-surveyed basin below sea level in East Antarctica, *Geophys. Res. Lett.*, 35, L16503, doi:10.1029/2008GL034728, 2008.
- Le Brocq, A. M., Payne, A. J., Siegert, M. J., and Alley, R. B.: A subglacial water-flow model for West Antarctica, *J. Glaciol.*, 55, 879–888, 2009.
- Le Brocq, A. M., Payne, A. J., and Vieli, A.: An improved Antarctic dataset for high resolution numerical ice sheet models (ALBMAP v1), *Earth Syst. Sci. Data*, 2, 247–260, doi:10.5194/essd-2-247-2010, 2010.
- Le Brocq, A. M., Bentley, M. J., Hubbard, A., Fogwill, C. J., Sugden, D. E., and Whitehouse, P. L.: Reconstructing the last glacial maximum ice sheet in the Weddell Sea embayment, Antarctica, using numerical modeling constrained by field evidence, *Quat. Sci. Rev.*, 30, 2422–2432, 2011.
- Lingle, C., Bueler, E., Brown, J., and Covey, D.: PISM, a Parallel Ice Sheet Model: current status of our Antarctic ice sheet simulation, JPL PARCA meeting, 29–31 January, 2007, available online: http://www2.gi.alaska.edu/snowice/glaciers/iceflow/parcaslides_JAN07.pdf, 2007.
- Lythe, M. B., Vaughan, D. G., and the BEDMAP Consortium: BEDMAP: a new ice thickness and subglacial topographic model of Antarctica, *J. Geophys. Res.* 106(B6), 11335–11351, 2001.
- MacAyeal, D. R.: The basal stress distribution of ice stream E, Antarctica, inferred by control methods, *J. Geophys. Res.*, 97, 595–603, 1992.
- MacAyeal, D. R.: A tutorial on the use of control methods in ice-sheet modeling, *J. Glaciol.*, 39, 91–98, 1993.
- MacAyeal, D. R. and Thomas, R. H.: The effects of basal melting on the present flow of the Ross ice shelf, Antarctica, *J. Glaciol.*, 32, 72–83, 1986.
- Marshall, S. J., Clarke, G. K. C., Dyke, A. S., and Fisher, D. A.: Geologic and topographic controls on fast flow in the Laurentide and Cordilleran ice sheets, *J. Geophys. Res.*, 101, 17827–17839, 1996.
- Morlighem, M., Rignot, E., Seroussi, H., Larour, E., Ben Dhia, H., and Aubry, D.: Spatial patterns of basal drag inferred using control methods from a full-Stokes and sim-

Distribution of basal sliding coefficients under ice sheets

D. Pollard and
R. M. DeConto

Title Page

Abstract

Introduction

Conclusions

References

Tables

Figures

◀

▶

◀

▶

Back

Close

Full Screen / Esc

Printer-friendly Version

Interactive Discussion

pler models for Pine Island Glacier, West Antarctica, *Geophys. Res. Lett.*, 37, L14502, doi:10.1029/2010GL043853, 2010.

Oerlemans, J. and Nick, F. M.: Modelling the advance-retreat cycle of a tidewater glacier with simple sediment dynamics, *Glob. Plan. Change*, 50, 148–160, 2006.

Pattyn, F.: Antarctic subglacial conditions inferred from a hybrid ice sheet/stream model, *Earth Plan. Sci. Lett.*, 295, 451–461, 2010.

Pattyn, F., Schoof, C., Perichon, L., Hindmarsh, R. C. A., Bueler, E., de Fleurian, B., Durand, G., Gagliardini, O., Gladstone, R., Goldberg, D., Gudmundsson, G. H., Lee, V., Nick, F. M., Payne, A. J., Pollard, D., Rybak, O., Saito, F., and Vieli, A.: Results of the Marine Ice Sheet Model Intercomparison Project, *MISMIP, The Cryosphere Discuss.*, 6, 267–308, doi:10.5194/tcd-6-267-2012, 2012.

Peters, L. E., Anandakrishnan, S., Alley, R. B., Winberry, J. P., Voigt, D. E., Smith, A. M., and Morse, D. L.: Subglacial sediments as a control on the onset and location of two Siple Coast ice streams, West Antarctica, *J. Geophys. Res.*, 111, B01302, doi:10.1029/2005JB003766, 2006.

Philippon, G., Ramstein, G., Charbit, S., Kageyama, M., Ritz, C., and Dumas, C.: Evolution of the Antarctic ice sheet throughout the last deglaciation: a study with a new coupled climate-north and south hemisphere ice sheet model, *Earth Plan. Sci. Lett.*, 248, 750–758, 2006.

Pimentel, S., Flowers, G. E., and Schoof, C. G.: A hydrologically coupled higher-order flow-band model of ice dynamics with a Coulomb friction sliding law, *J. Geophys. Res.*, 115, F04023, doi:10.1029/2009JF001621, 2010.

Pollard, D. and DeConto, R. M.: Antarctic ice and sediment flux in the Oligocene simulated by a climate-ice sheet-sediment model, *Palaeogeogr. Palaeoclim. Palaeoecol.*, 198, 53–67, 2003.

Pollard, D. and DeConto, R. M.: A coupled ice-sheet/ice-shelf/sediment model applied to a marine-margin flowline: forced and unforced variations, in: *Glacial Sedimentary Processes and Products*, Hambrey, M. J., Christoffersen, P., Glasser, N. F., and Hubbard, B., *Int. Assoc. of Sedimentol. Special Publ.* 39, Blackwell, Oxford, UK, 37–52, 2007.

Pollard, D. and DeConto, R. M.: Modelling West Antarctic ice sheet growth and collapse through the past five million years, *Nature*, 458, 329–332, 2009.

Pollard, D. and DeConto, R. M.: Formulation of a hybrid ice sheet-stream-shelf model, applied to Antarctica, *Geosci. Model Dev. Discuss.*, submitted, 2012.

Distribution of basal sliding coefficients under ice sheetsD. Pollard and
R. M. DeConto

Title Page

Abstract

Introduction

Conclusions

References

Tables

Figures

◀

▶

◀

▶

Back

Close

Full Screen / Esc

Printer-friendly Version

Interactive Discussion



- Price, S. F., Payne, A. J., Howat, I. M., and Smith, B. E.: Committed sea-level rise for the next century from Greenland ice sheet dynamics during the past decade, *P. Natl. Acad. Sci.*, 108, 8978–8993, 2011.
- Raymond Pralong, M. and Gudmundsson, G. H.: Bayesian estimation of basal conditions on Rutford ice stream, West Antarctica, from surface data, *J. Glaciol.*, 57, 315–324, 2011.
- Rignot, E., Mouginot, J., and Scheuchl, B.: Ice flow of the Antarctic ice sheet, *Science*, 333, 1428–1430, 2011.
- Ritz, C., Rommelaere, V., and Dumas, C.: Modeling the evolution of Antarctic ice sheet over the last 420 000 years: implications for altitude changes in the Vostok region, *J. Geophys. Res.*, 106, 31943–31964, 2001.
- Schoof, C.: The effect of cavitation on glacier sliding, *Proc. R. Soc. Ser. A.*, 461, 609–627, 2005.
- Schoof, C.: Ice sheet grounding line dynamics: steady states, stability, and hysteresis, *J. Geophys. Res.*, 112, F03S28, doi:10.1029/2006JF000664, 2007.
- Shapiro, N. M. and Ritzwoller, M. H.: Inferring surface heat flux distributions guided by a global seismic model: particular application to Antarctica, *Earth Plan. Sci. Lett.*, 223, 213–224, 2004.
- Stone, E. J., Lunt, D. J., Rutt, I. C., and Hanna, E.: Investigating the sensitivity of numerical model simulations of the modern state of the Greenland ice-sheet and its future response to climate change, *The Cryosphere*, 4, 397–417, doi:10.5194/tc-4-397-2010, 2010.
- Studinger, M., Bell, R. E., Blankenship, D. D., Finn, C. A., Arko, R. A., Morse, D. L., and Joughin, I.: Subglacial sediments: a regional geological template for ice flow in West Antarctica, *Geophys. Res. Lett.*, 28, 3493–3496, 2001.
- Tarasov, L., Dyke, A. S., Neal, R. M., and Peltier, W. R.: A data-calibrated distribution of deglacial chronologies for the North American ice complex from glaciological modeling, *Earth Plan. Sci. Lett.*, 315–316, 30–40, 2012.
- Thomas, I. D., King, M. A., Bentley, M. J., Whitehouse, P. L., Penna, N. T., Williams, S. D. P., Riva, R. E. M., Lavallee, D. A., Clarke, P. J., King, E. C., Hindmarsh, R. C. A., and Koivula, H.: Widespread low rates of Antarctic glacial isostatic adjustment revealed by GPS observations, *Geophys. Res. Lett.*, 38, L22302, doi:10.1029/2011GL049277, 2011.
- Tulaczyk, S., Kamb, B., Scherer, R. P., and Engelhardt, H. F.: Sedimentary processes at the base of a West Antarctic ice stream: constraints from textural and compositional properties of subglacial debris, *J. Sedim. Res.*, 68, 487–496, 1998.

Distribution of basal sliding coefficients under ice sheets

D. Pollard and
R. M. DeConto

Title Page

Abstract

Introduction

Conclusions

References

Tables

Figures

⏪

⏩

◀

▶

Back

Close

Full Screen / Esc

Printer-friendly Version

Interactive Discussion



- Van de Berg, W. J., van den Broeke, M. R., and van Meijgaard, E.: Reassessment of the Antarctic surface mass balance using calibrated output of a regional atmospheric climate model, *J. Geophys. Res.*, 111, D11104, doi:10.1029/2005JD006495, 2006.
- 5 Vielei, A. and Payne, A. J.: Application of control methods for modelling the flow of Pine Island Glacier, West Antarctica, *Ann. Glaciol.*, 36, 197–204, 2003.
- Young, D. A., Wright, A. P., Roberts, J. L., Warner, R. C., Young, N. W., Greenbaum, J. S., Schroeder, D. M., Holt, J. W., Sugden, D. E., Blankenship, D. D., van Ommen, T. D., and Siegert, M. J.: A dynamic early East Antarctic ice sheet suggested by ice-covered fjord landscapes, *Nature*, 474, 72–75, 2011.
- 10 Wang, W. L. and Warner, R. C.: Modelling of anisotropic ice flow in Law Dome, East Antarctica, *Ann. Glaciol.*, 29, 184–190, 1999.
- Whitehouse, P. L., Bentley, M. J., and Le Brocq, A. M.: A deglacial model for Antarctica: geological constraints and glaciological modeling as a basis for a new model of Antarctic glacial isostatic adjustment, *Quaternary Sci. Rev.*, 32, 1–24, 2012.

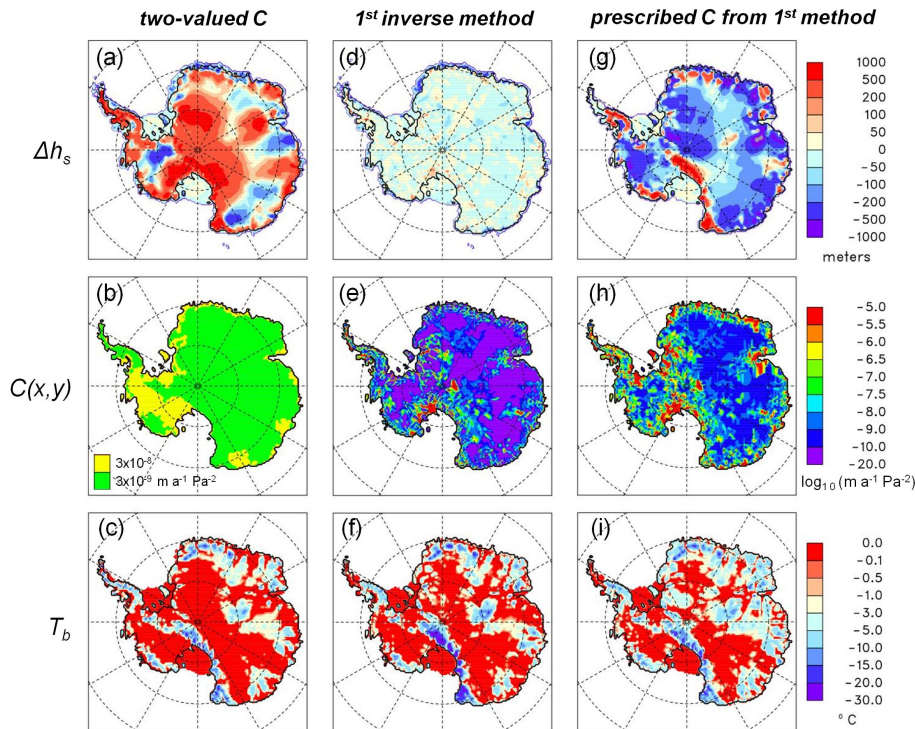


Fig. 1. Top row: model minus observed surface ice elevation errors (m). Middle row: basal sliding coefficients $C(x,y)$, $\log_{10}(\text{m a}^{-1} \text{Pa}^{-2})$. Bottom row: homologous basal temperatures T_b (relative to pressure-melt point) ($^{\circ}\text{C}$). Left column (a–c) with prescribed two-value $C(x,y)$ according to whether rebounded ice-free bed elevations are above or below sea level. Middle column (d–f) using first inverse method (no effect of T_b on sliding). Right column (g–i) non-inverse run with prescribed nearest-neighbor-filled $C(x,y)$ from first method.

Distribution of basal sliding coefficients under ice sheets

D. Pollard and R. M. DeConto

Title Page

Abstract Introduction

Conclusions References

Tables Figures

◀ ▶

◀ ▶

Back Close

Full Screen / Esc

Printer-friendly Version

Interactive Discussion



Distribution of basal sliding coefficients under ice sheets

D. Pollard and
R. M. DeConto

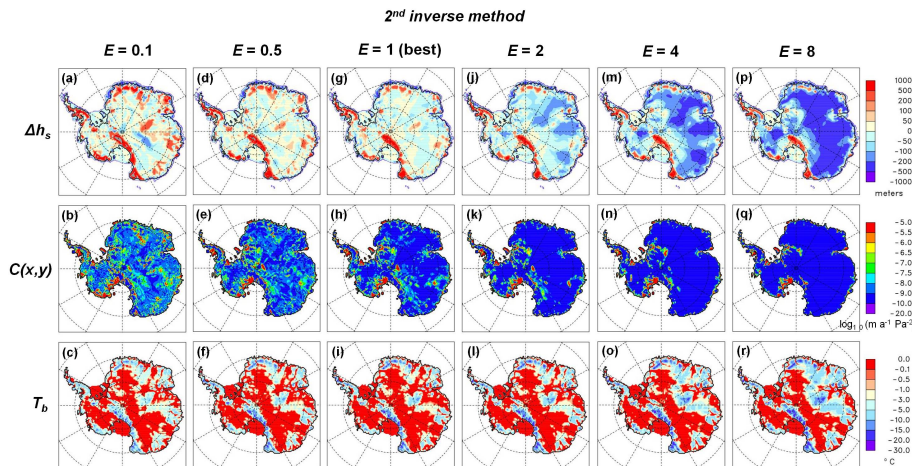


Fig. 2. Top row: model minus observed surface ice elevation errors (m). Middle row: basal sliding coefficients $C(x, y)$, $\log_{10} (\text{m a}^{-1} \text{Pa}^{-2})$. Bottom row: homologous basal temperatures T_b ($^{\circ}\text{C}$). Each column shows results using second inverse method (T_b affecting sliding) for a different value of the internal-flow enhancement factor E , ranging from $E = 0.1$ to $E = 8$.

[Title Page](#)
[Abstract](#)
[Introduction](#)
[Conclusions](#)
[References](#)
[Tables](#)
[Figures](#)
[⏪](#)
[⏩](#)
[◀](#)
[▶](#)
[Back](#)
[Close](#)
[Full Screen / Esc](#)
[Printer-friendly Version](#)
[Interactive Discussion](#)

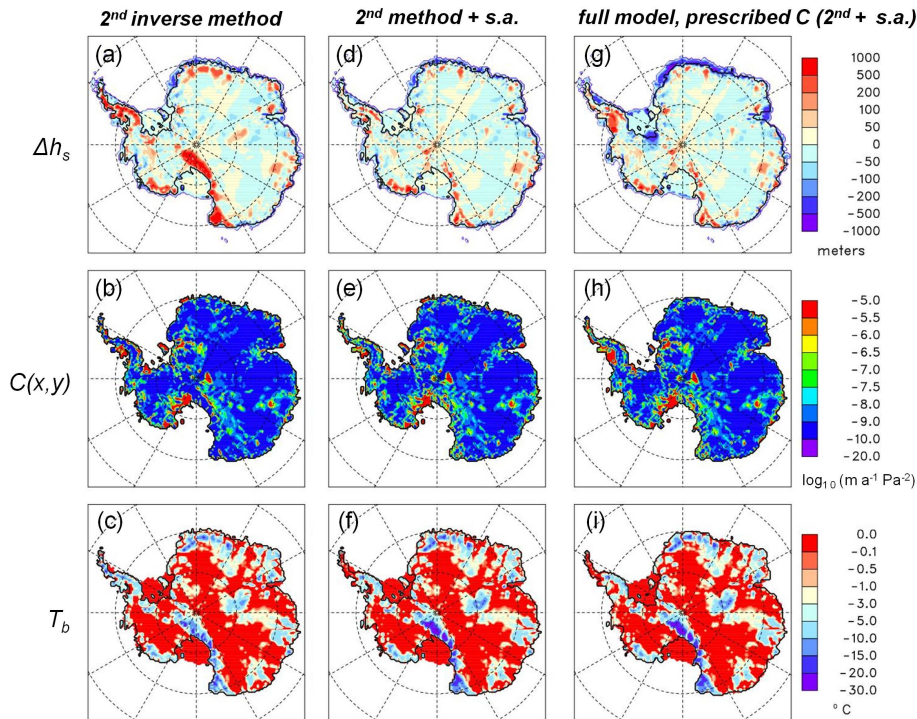


Fig. 3. Top row: model minus observed surface ice elevation errors (m). Middle row: basal sliding coefficients $C(x,y)$, $\log_{10}(\text{m a}^{-1} \text{Pa}^{-2})$. Bottom row: homologous basal temperatures T_b (°C). Left column (a–c) using second inverse method (T_b affecting sliding), as in Fig. 2g–i. Middle column (d–f) using second inverse method with additional sub-grid topographic effect on sliding. Right column (g–i) non-inverse run with prescribed $C(x,y)$ from second method with sub-grid topographic effect, and freely varying grounding lines and ice sheets.

Distribution of basal sliding coefficients under ice sheets

D. Pollard and
R. M. DeConto

Title Page

Abstract

Introduction

Conclusions

References

Tables

Figures

◀

▶

◀

▶

Back

Close

Full Screen / Esc

Printer-friendly Version

Interactive Discussion

Distribution of basal sliding coefficients under ice sheets

D. Pollard and
R. M. DeConto

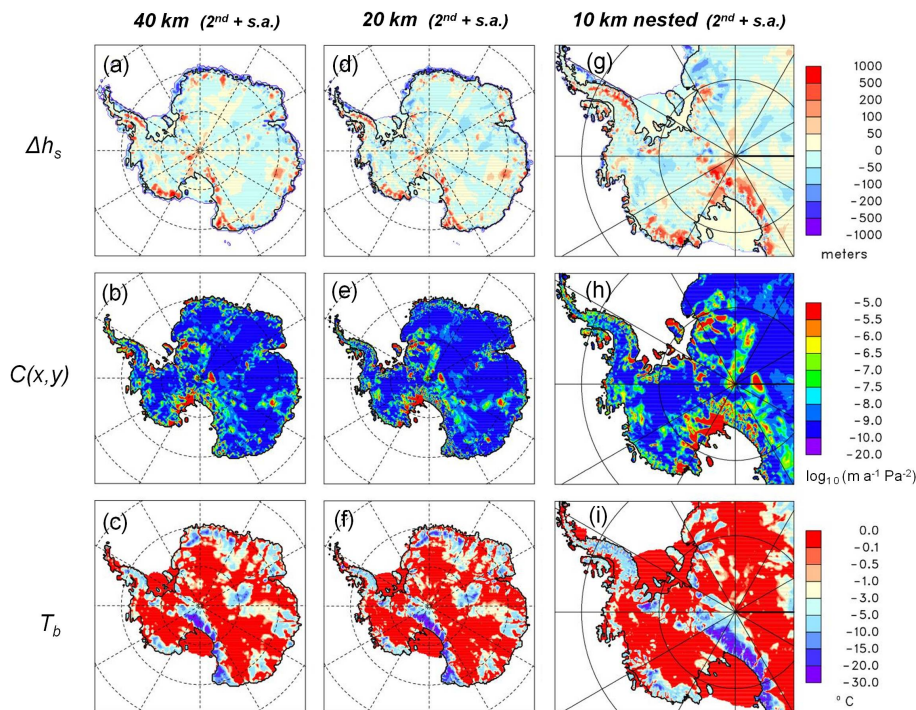


Fig. 4. Top row: model minus observed surface ice elevation errors (m). Middle row: basal sliding coefficients $C(x,y)$, $\log_{10}(\text{m a}^{-1} \text{Pa}^{-2})$. Bottom row: homologous basal temperatures T_b ($^{\circ}\text{C}$). Left column (a–c) using second inverse method with sub-grid topographic effect, 40 km resolution (as in Fig. 3d–f). Middle column (d–f) as left, except 20 km resolution. Right column (g–i) as left, except limited-domain nested run at 10 km resolution, with lateral boundary conditions from corresponding 20-km run.

Title Page

Abstract

Introduction

Conclusions

References

Tables

Figures

◀

▶

◀

▶

Back

Close

Full Screen / Esc

Printer-friendly Version

Interactive Discussion

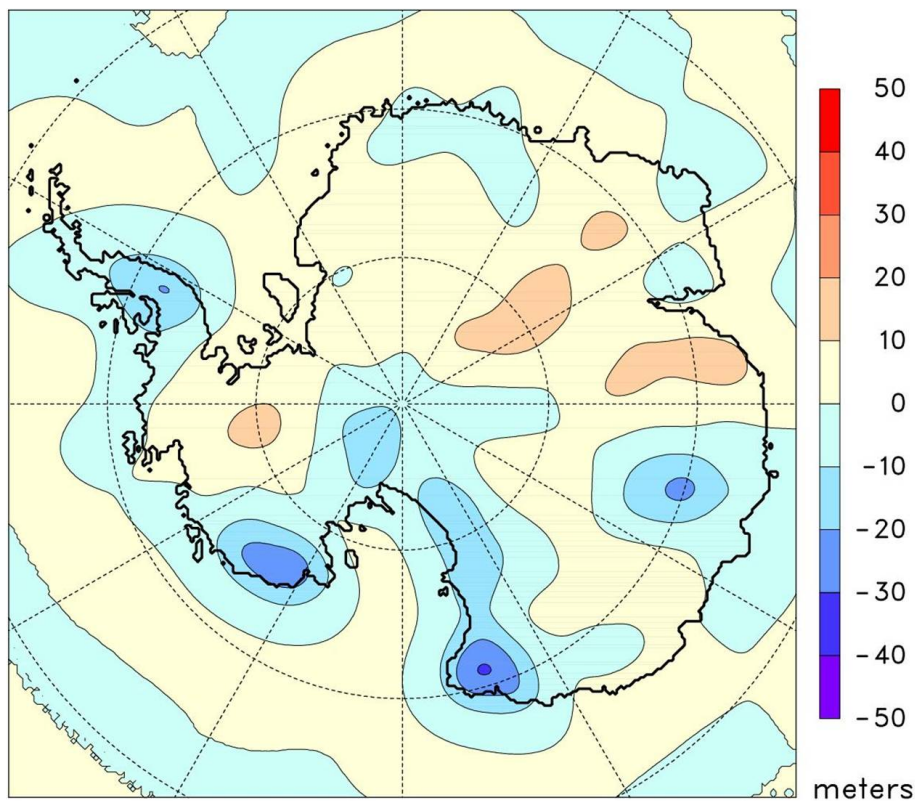


Fig. A1. Model minus observed modern bed elevations, meters, using second inverse method with sub-grid topographic effect, 20 km resolution (as in Fig. 4d–f).

Distribution of basal sliding coefficients under ice sheets

D. Pollard and
R. M. DeConto

Title Page

Abstract Introduction

Conclusions References

Tables Figures

◀ ▶

◀ ▶

Back Close

Full Screen / Esc

Printer-friendly Version

Interactive Discussion

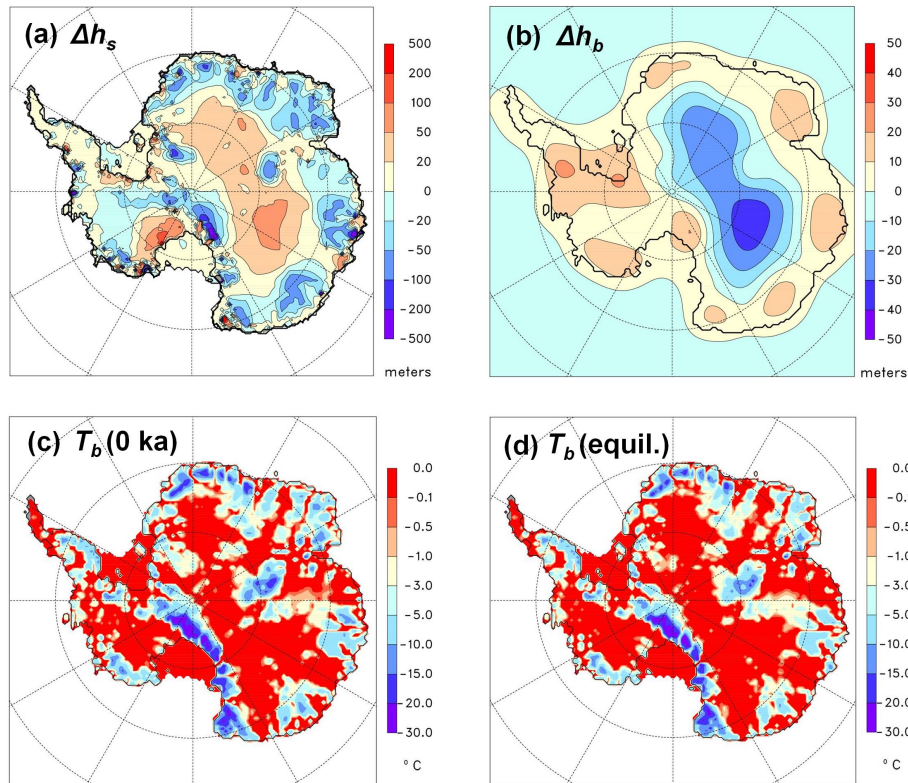


Fig. B1. (a) Difference in ice surface elevations (m), equilibrated run with invariant modern forcing minus 0 ka snapshot from a transient run through the last 80 kyr. Both runs used prescribed basal coefficients $C(x, y)$, sliding affected by basal temperature and sub-grid topography, and freely varying grounding lines and ice shelves (as in Fig. 3g–i). (b) As (a) except difference in bed elevations. (c) Homologous basal temperature ($^{\circ}\text{C}$) for transient run at 0 ka. (d) As (c) except for equilibrated run.

Distribution of basal sliding coefficients under ice sheets

D. Pollard and
R. M. DeConto

Title Page

Abstract

Introduction

Conclusions

References

Tables

Figures

◀

▶

◀

▶

Back

Close

Full Screen / Esc

Printer-friendly Version

Interactive Discussion

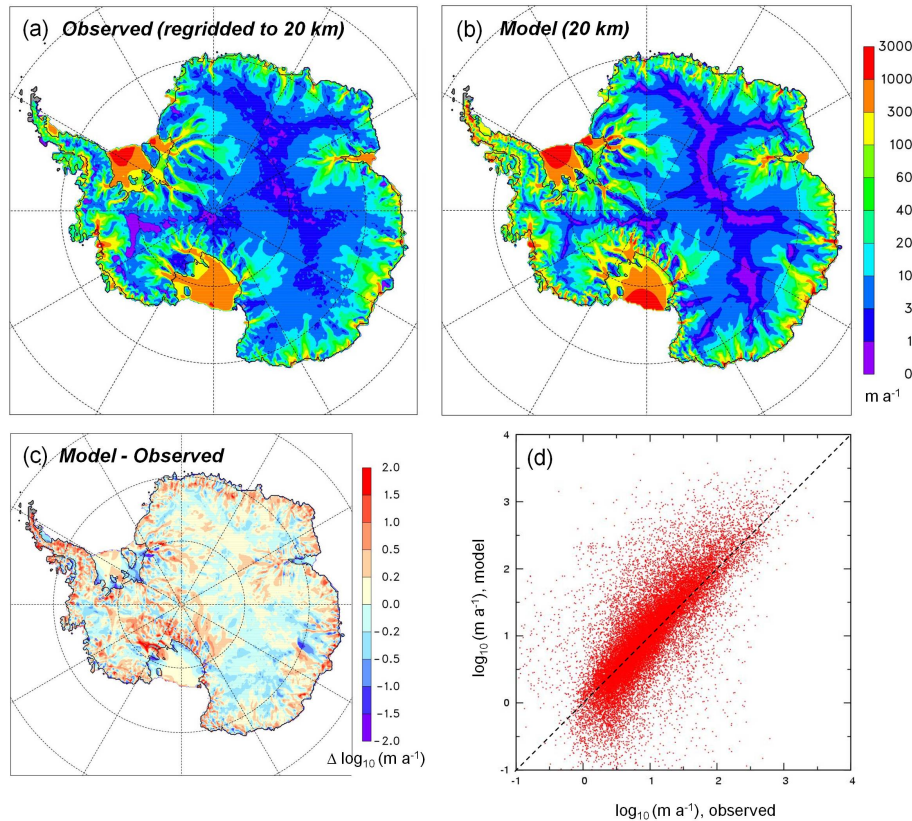


Fig. C1. (a) Observed surface ice velocity (Rignot et al., 2011), averaged here to 20 km model cells (m a^{-1}). (b) Model surface ice velocity (m a^{-1}), using second inverse method with sub-grid topographic effect, 20 km resolution (as in Fig. 4d–f). (c) Model minus observed velocity, difference in $\log_{10}(\text{m a}^{-1})$, i.e., $\log_{10}(v_{\text{model}}/v_{\text{observed}})$, with imposed minimum of 2 m a^{-1} . (d) scatter plot of observed vs. model velocities ($\log_{10}(\text{m a}^{-1})$) for each 20-km grid cell with grounded ice.

Distribution of basal sliding coefficients under ice sheets

D. Pollard and
R. M. DeConto

Title Page

Abstract Introduction

Conclusions References

Tables Figures

⏪ ⏩

◀ ▶

Back Close

Full Screen / Esc

Printer-friendly Version

Interactive Discussion



Distribution of basal sliding coefficients under ice sheets

D. Pollard and
R. M. DeConto

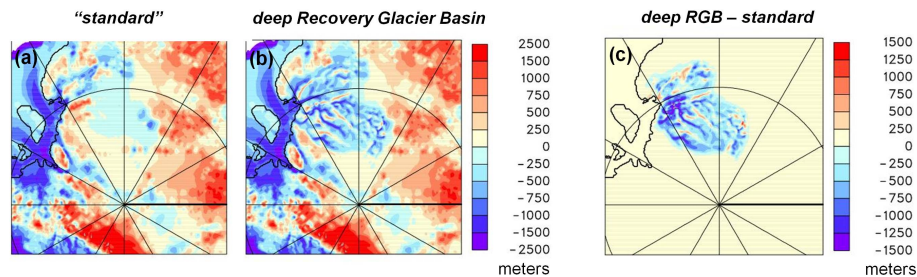


Fig. D1. (a) Modern bed elevations, meters (ALBMAP, Le Brocq et al., 2010), averaged here to 10-km model cells. (b) As (a) except with deeper topography in the Recovery Glacier catchment area (m), (ibid; Le Brocq et al., 2008). (c) Difference (b) minus (a).

[Title Page](#)
[Abstract](#)
[Introduction](#)
[Conclusions](#)
[References](#)
[Tables](#)
[Figures](#)
[⏪](#)
[⏩](#)
[◀](#)
[▶](#)
[Back](#)
[Close](#)
[Full Screen / Esc](#)
[Printer-friendly Version](#)
[Interactive Discussion](#)


Distribution of basal sliding coefficients under ice sheets

D. Pollard and
R. M. DeConto

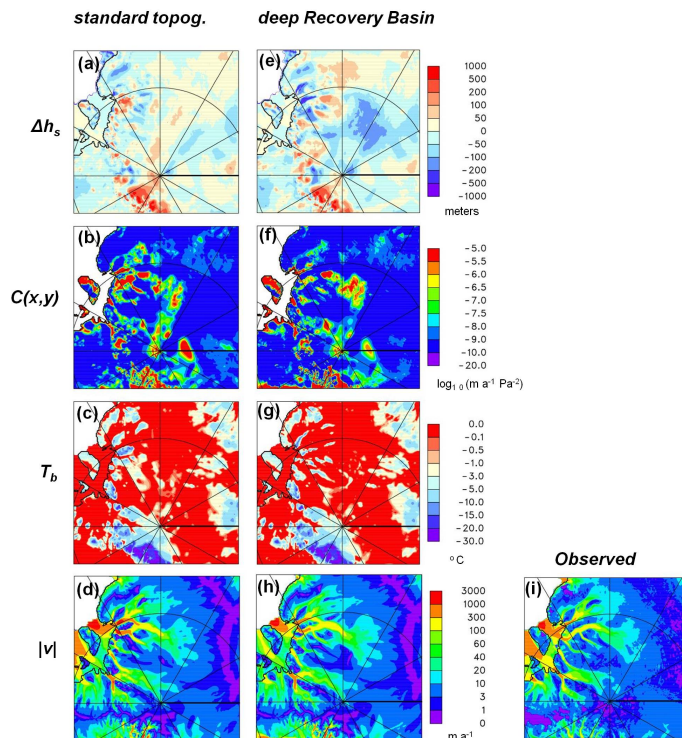


Fig. D2. Top row: model minus observed surface ice elevation errors (m). Second row: basal sliding coefficients $C(x,y)$, $\log_{10}(\text{m a}^{-1} \text{Pa}^{-2})$. Third row: homologous basal temperatures T_b ($^{\circ}\text{C}$). Bottom row: surface ice velocity (m a^{-1}). Left column (**a–d**) using second inverse method with sub-grid topographic effect, limited-domain nested run at 10 km resolution with lateral boundary conditions from corresponding continental run. Middle column (**e–h**) as left, except using alternate bed topography with deeper elevations in Recovery Glacier drainage basin (Le Brocq et al., 2008). Right column (**i**) Observed surface ice velocity (Rignot et al., 2011), averaged here to 10 km model cells (m a^{-1}).